Article

Design and Implementation of Extremum-Seeking Control Based on MPPT for Dual-Axis Solar Tracker

Cesar Ulises Solís-Cervantes [1], Sergio Isai Palomino-Resendiz [2,*], Diego Alonso Flores-Hernández [3], Marco Antonio Peñaloza-López [3] and Carlos Manuel Montelongo-Vazquez [2]

1 Automatic Control Department, CINVESTAV-IPN, Av. Instituto Politecnico Nacional 2508, Col. San Pedro Zacatenco, Mexico City C.P. 07360, Mexico; cesar.solis@cinvestav.mx
2 Automation and Control Engineering Department, ESIME-IPN, Unidad Profesional Adolfo López Mateos, Zacatenco, Av. Luis Enrique Erro s/n, Mexico City C.P. 07738, Mexico; cmontelongov@ipn.mx
3 Instituto Politécnico Nacional UPIITA, Mexico City C.P. 07340, Mexico; dfloreshe@ipn.mx (D.A.F.-H.); mpenalozal1500@alumno.ipn.mx (M.A.P.-L.)
* Correspondence: spalominor@ipn.mx

Abstract: The increase in the production efficiency of photovoltaic technology depends on its alignment in relation to the solar position. Solar tracking systems perform the tracking action by implementing control algorithms that help the reduction of tracking errors. However, conventional algorithms can reduce the life of actuators and mechanisms due to control action, significantly reducing operation times and profitability. In this article, an unconventional control scheme is developed to address the mentioned challenges, presenting the design and implementation of an extremum-seeking control to perform maximum power point tracking for a two-axis solar tracker instrumented with a solar module. The proposed controller is governed by the dynamics of a classic proportional-integral scheme and assisted by sensorless feedback. Also, it has an anti-wind-up-type configuration for the integral component and counts with a variable amplitude for the dither signal. The proposal is validated experimentally by comparison between a fixed system and a two-axis system in azimuth-elevation configuration. In addition, two performance indices are defined and analyzed, system energy production and tracking error. The results show that the proposal allows producing up to 27.75% more than a fixed system, considering the tracker energy consumption due to the tracking action and a pointing accuracy with $\pm 1.8°$ deviation. Finally, an analysis and discussion are provided based on the results, concluding that the proposed algorithm is a viable alternative to increase the performance of tracked photovoltaic systems.

Keywords: extremum-seeking control; MPPT; solar tracker; solar energy; solar cells

MSC: 49N05; 93-05; 90-05; 70E60; 37-04

1. Introduction

Solar energy has become a global trend due to the benefits it provides in terms of sustainability [1]. Today, of the total energy consumed in the world, solar energy contributes 8% and it is estimated that in the coming decades, along with other clean sources, it will replace conventional sources obtained mainly from fossil fuels [2]. To take advantage of solar energy, it is necessary to subject it to a capture and conversion process through the use of specialized devices such as solar cells (SCs) and optical concentrators, among others [3].

The principle operation of the devices consists of its simple exposure to solar radiation, but to obtain its best productive efficiency, the orientation of its collection surface towards the sun must be guaranteed with some precision as its trajectory evolves, as well as good weather conditions (sunny and clear days) [4]. For this reason, it is common to resort to the use of solar tracking (ST) systems capable of performing the tasks of pointing at the

capturing surface of the devices automatically. This is by mechanisms that reproduce the solar trajectory through controlled movements in the azimuthal and elevation axis [5].

In general, optical devices for solar concentration and hybrid systems increase electrical energy production due to the conversion efficiency of the photovoltaic cells compared to conventional photovoltaic technology. However, they require high tracking precision with an error less than 0.5° and clear-sky environmental conditions due to the optical elements [6]. Consequently, systems with conventional photovoltaic modules are used more frequently since they operate uninterruptedly regardless of weather conditions. These systems are classified into high and low operating regimes. The first generates the greatest amount of energy, requiring a pointing error less than 2°. And the energy production of the second regime is proportional to the configured fixed alignment and the luminous intensity [4]. The production value can be affected to the point of compromising its profitability, either due to the energy consumption involved in the operation of the ST or due to configuration and maintenance tasks in the short and long term [7]. In this way, on a global energy production scale, such as solar farms, the fixed configurations of SCs are used, reducing the capacity of production. Consequently, to meet production objectives and compensate for the losses due to fixed configuration, the collection surface is increased considerably [8].

The integration of STs into systems using SCs promises to achieve up to 48% higher energy production compared to fixed SC configurations. However, in reality the final production value is lower and even negative [9], since the energy consumption involved in the operation of the ST, or the development of configuration and maintenance tasks (short and long term) [7], must be taken into account. Therefore, it is obvious why fixed SC configurations are used globally in large-scale energy-production applications, such as so-called solar farms, and to meet production targets or compensate for losses resulting from constant deviation the collection surface is increased with more SCs [8].

In the short term, the above can be seen as a simple and practical plan to harness the benefits of solar energy. However, today this represents a big problem in terms of pollution since there are currently no profitable and sustainable processes that allow 100% of the components of an SC to be recovered once its useful life has ended (which is approximately 10–15 years). Furthermore, in this same aspect there are no formal regulations for the use and/or management of the waste generated by [10]. This takes into consideration that second and/or third-generation SCs are used in most solar plants, that is, devices made from gallium, germanium and, to a greater extent, silicon [11]. On the other hand, it must also be taken into account that the surfaces of solar plants usually cover hundreds of hectares, which has negative effects on ecosystems, as well as on their biodiversity [12]. According to [13], it is estimated that by 2050 there will be 78 million tons of toxic waste as a result of the use of this type of energy-production scheme. Today, it is not possible to deactivate solar plants since in each country in which they are used they provide a significant amount of energy. Therefore, in this work, it is proposed to reduce the collection surface through the use of STs that guarantee a profitable operation. Thus, the amount of energy production (which should be greater than a fixed configuration) will be proportional to the surface that can be eliminated and consequently to the problems that this represents.

In recent years, important advances have been reported in the literature for the design and operation of STs based on mechatronic and optimization philosophies [14,15]. Where, the objectives of the methodologies focus mainly on improving aspects related to their mechanisms, control laws and management of solar trajectories. In this way, aspects such as robustness, mobility, precision, energy consumption and degree of automation, among other things, benefit. In other words, given the use of the methodologies, it is guaranteed that the profitability of the ST will be positive. However, in reality, most STs are designed under the premise of the operation of classic and simple control schemes (such as On-Off or PID), which are mainly associated with the development of solar tracking tasks with high precision. This, is regardless of profitability, since, in general, this type of

controller is chosen for aspects such as ease of development, implementation, operation, adjustment and calibration, as well as low economic costs [16].

To reduce the disadvantages and limitations of the controllers normally used in STs, some authors present alternatives that are based on optimization methods to improve their performance [17–19]. For example, maximum power point tracking (MPPT) is used, a method focused on trajectory management to achieve the maximum production rate of the SC at each instant [20–22]. From the above, the developments of controlled movements on the axes of the ST are evident; they are calculated based on the measurement and processing of one or more parameters associated with the components of the solar rays (such as the value of irradiance, temperature, luminosity) [23–26]. And as a special configuration called sensorless, the above can also be achieved by measuring and processing the value of the energy produced by the SC in terms of electrical energy, or some of its components such as current [27].

A review of at least 80 proposals for sensor arrays and their configurations, which are mainly used in MPPT applications, is presented in [28]. In these alternatives, it is clear that having a greater number of sensors increases the pointing precision and this translates positively into the amount of energy that the SC can produce. However, it is a fact that the use of more sensors implies increasing the processing and instrumentation requirements associated with the operation of the ST and consequently the profitability of each proposal may be compromised. Furthermore, in works such as [29,30] two alternatives are presented that are helped by the basic form of the controllers that govern this type of scheme, which allows us to notice that the calculation of control efforts is still motivated by the follow trajectories with great precision regardless of the energy consumption that may entail, which negatively translates into profitability. On the other hand, [31] presents an analysis of at least 20 proposals of the benefits of using non-conventional schemes based on adaptation laws, neural networks, fuzzy logic and genetic algorithms, for tuning classical PID-type controllers used in MPPT. According to their results, it is possible to solve the limitations and problems presented by conventional methods. However, it is important to mention that this type of option involves the use of complex numerical methods and that in many cases they belong to software available under license and with high computational cost, increasing the complexity of the problem and the cost of the final application.

Thus, to avoid all of the above, the MPPT can use a scheme based on ESC [32,33], a methodology that consists of carrying out the process of maximizing a function by calculating the Hessian of a modulated signal, which is built in real-time and governs the movements of the actuators that are developed. The modulated signal corresponds to the dynamics of the current generated by the SC and its interaction with a sinusoidal-type signal (called dither) that allows obtaining an oscillating behavior around the real value [34,35]. This makes it possible to dispense with the use of more sensors and since the algorithm can be solved analytically, the use of reserved numerical methods is avoided. Furthermore, its basic operation is implemented in control schemes mainly of the PI type, so the degree of complexity does not increase significantly [36]. Although there are variations in which other types of alternatives can be integrated, such as Model-Based Predictive Control, the design of robust systems under the Lyapunov methodology, active disturbance rejection and artificial neural networks, among others [37–41].

In the literature [42], ESC, mainly in its basic configuration [43–45], is considered as a fairly competitive alternative to MPPT assistance, since its performance projection promises a significant increase in energy production, guaranteeing convergence to the optimum, ease of configuration, etc. However, in practice this is not very convincing, since although in most applications a high orientation accuracy is demonstrated (greater than 99.9% towards the sun), it is also easy to notice that the energy consumption involved in the performance of the ST has little relevance, which can constitute a compromise in the profitability of its application. Then, works such as [41,46] present special ESC configurations (in simulation and laboratory environments, respectively) to improve the operating response under adverse weather conditions and, although the results are favorable, it must be understood

that the dynamics used ignore a host of effects that can affect the ST and its components in reality.

From the above, it can be established that in general terms, the variations and contributions of the ESC in ST lie in the way of constructing the modulated signal and/or the design of filters. Therefore, the energy consumption involved is of little relevance, although the nature of the ESC implies maintaining a permanent oscillatory movement. In addition, no proposal takes into account that although the controller has a very simple form, it is important to consider that the integral action can cause negative effects in the long term, such as memory overflow or exceeding the permissible limits of the actuators. Therefore, implementing it in the development of a task that in favorable conditions can take up to 12 h of operation (from sunrise to sunset) is practically incompatible.

Thus, for all the above reasons, this proposal presents the development and implementation of an ESC capable of satisfying the main motivation, as well as the problems commonly related to its implementation in ST. That is, the performance of the ESC must exceed the energy-production capacity of a fixed system in real terms since, as previously established, the increase in production is proportional to the recoverable surface in solar parks. Regarding the design, development and implementation of the ESC for an existing ST, the following contributions are made:

- Development and experimentation of a novel control strategy for two-axis tracking systems to increase the energy production of conventional photovoltaic technology through the reduction of tracking error based on extremum-seeking control in its basic form.
- Development and testing of dynamic dither signal-management system, adjusting the amplitude of the dither signal based on the calculations of the optimization process, modifying the value concerning the operating conditions of every moment. Thus, instead of performing permanent movements with constant amplitude on the axes consuming unnecessary energy, movement decisions are interpreted only in a virtual environment and executed in reality if necessary.
- Development of an anti-wind-up configuration for PI controller to avoid saturation of the scaling actions of an integral part and obtain behaviors that may affect the actuators, based on saturation and cleaning operations of the integral gain every certain period during operation.

Finally, the proposal opens the way to new developments and research to increase the energy gain of conventional photovoltaic systems with solar tracking through the development of non-conventional control strategies that allow for optimization of the solar collection area in relation to the production capacity. The work is presented as follows. Section 2 provides an overview of the ST used for this case study, and the modeling of the SC and the formulation of the ESC. Then, Section 3 contains the development of an experimental methodology that allows validating and evaluating the performance of the ESC, as well as an analysis and discussion of the graphical and/or numerical results. Finally, Section 4 provides conclusions and proposals for future work.

2. Preliminaries

2.1. Solar Tracker Description

Figure 1 shows the ST used for this work, which has dimensions of $200 \times 200 \times 300$ mm in its workspace. In the azimuthal and elevation axis, the mechanisms were built with a hollow aluminum structural profile (T-6061) to reduce weight without losing resistance to deformation due to loads and stresses and each one uses a DC motor with gear reducer model SKU 5203-2402-0188. Then, in the lower part of the ST structure, with dimensions $200 \times 200 \times 150$ mm, there is a compartment that serves to protect the elements of the power stage and the acquisition and processing instruments of signals, which are made up of a 6 *W* power supply (12 V—0.5 A), an STM32 Nucleo-F411RE microcontroller, a current sensor model LTS 15-NP and a dual driver motor model VNH2SP30. On the other hand,

the ST has an SC with dimensions of $360 \times 550 \times 25$ mm, an average weight of 1.5 kg and a nominal production rate of 25 W (i.e., 17.45 V—1.43 A).
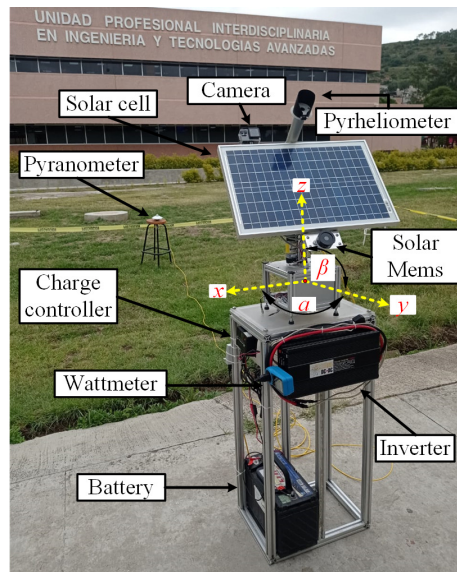

Figure 1. General graphic description of solar tracker.

Additionally, as a complement to the monitoring and validation of its performance, a pyrheliometer, a camera and a Solar Mems can be observed in the structure of the SC and a pyranometer is located at a certain distance from the structure. It is worth mentioning that the system has a certain degree of autonomy and during its operation it does not need to be connected to a conventional power line. Therefore, in the lower structure that supports the ST, there is a charge controller, a wattmeter, a battery and an inverter. For more technical information about the ST, its components and connections, as well as manufacturing details, see [7,16].

2.2. SC Modeling and Problem Formulation

To model the SC, (1) can be used, a simplified model that describes the behavior of the current that is generated [47,48]. The model results from an analysis of the equivalent circuit presented in Figure 2.

$$i = i_p - i_o\left(e^{\frac{q(V+IR_s)}{p}} - 1\right) - \frac{V+IR_s}{R_{SH}} \tag{1}$$

where i_p is the generated photocurrent, i_o is the reverse saturation current and R_s and R_{SH} are the series and parallel resistance, respectively. Then, V is the resulting voltage, q the charge constant of an electron (with value 1.6×10^{-19} C) and p is a parameter that depends of the following equation

$$p = kT_c\xi$$

with k as the Boltzmann constant (with value 1.38×10^{-23} $\frac{J}{K}$), T_C the temperature of the SC and ξ is the ideality factor (which depends on the manufacturing material of the SC).
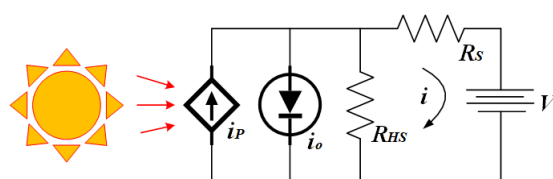

Figure 2. Equivalent circuit of the single diode model for SC.

Equation (1) provides an approximation that describes the dynamics of the SC. However, it must be clarified that its construction depends on the knowledge of its parameters, which can vary significantly during operation either due to the dynamics of the environment or due to wear of the SC. This represents a new problem and to avoid its implications, given that the current is a variable that can be measured and at the same time the production characteristics of the SC are known (through its datasheet), in this work we use a realistic model, which consists of using a model that expresses the dynamics of the current as a function of the luminosity flux received. The above involves the equivalence $i = \Phi$ [49,50]. Furthermore, in order not to ignore the effects of losses caused by deviations, operating conditions and current conditions of the cell (due to degradation of composition materials), among other things, in the relationship, a generalized variable Y is added, which can perform proportionality, that is

$$i = Y\Phi \tag{2}$$

In the literature, Y is a constant and takes values between 0.04 and 0.34 [51] and in general, this parameter is associated with the efficiency of capture and conversion of solar radiation that a photovoltaic-type device can have, or those used in concentration photovoltaic (CPV)-type applications [52]. For this work, Y $= 0.2039$ and its value was determined experimentally (see Appendix A). In addition, given that Φ is the received luminous flux, it is proposed that it take the form [53]

$$\Phi = \iint_C \bar{I} \cdot d\bar{S}$$

where $\bar{I}$ is the direction of the glare light wavefront (defined as I) and $d\bar{S}$ is a differential unit vector related to the surface S on which the light falls on the SC (whose shape is rectangular) and for this reason C in the integrals represents the bounded surface S. Thus, the model allows the problem to be directed to locating the orientation of maximum luminosity incidence through classic tracking tasks with the objective of moving the ST motors to maximize the incidence of light. For this reason, in the analysis and design of the controllers it is considered that the ST motors are part of the general dynamics of the SCs, since upon receiving the value of the angular reference (after processing the current value of the current) they execute real-time control efforts to update position. This is because in this scheme the SC is considered to be at the same time the sensor that feeds back to the control circuit (i.e., sensorless). On the other hand, given the purposes of the controller, it is proposed that the modeling of each motor be governed by a stable and decoupled MIMO-type transfer function, with which constant reference tracking is achieved [54]. That is

$$G(s) := \text{diag}\{G_1(s), G_2(s)\} \tag{3}$$

Such that

$$\lim_{s \to 0} G(s) = \mathbb{I}_2$$

where $G_1(s)$ and $G_2(s)$ can be considered as filters with cutoff frequencies ω_{c_1} and ω_{c_2}, respectively, and their inputs (α, β) are saturated by the angular constraints of each axis. That is, $\alpha \in [0, 2\pi]$ is the azimuthal angle (measured in the xy plane from the x axis) and $\beta \in [0, \frac{\pi}{2}]$ is the elevation angle (which is measured from the xy plane to the z axis). To identify the reference coordinates for the xyz planes, see Figure 2. Additionally, $\mathbb{I}_2 \in \mathbb{R}^{2\times 2}$ is an identity matrix. In that way, (2) takes the form

$$i(\alpha, \beta) = Y\Phi \tag{4}$$

Thus, for (4), if there is a single source of solar illumination whose wavefront is considered flat and oriented according to the vector $v_s = \begin{bmatrix} \alpha & \beta \end{bmatrix}^T$ with radiance I, this is a function of its angles (denoted by $v_0 = \begin{bmatrix} \alpha_0 & \beta_0 \end{bmatrix}^T$). So, if $v_0 \to v_s$ while $t \to \infty$, the current value

converges to the maximum. In addition, for the model it is considered that the SC has a reference vector that initially points to the coordinates $v_0 = (1, 0, 0)^T$ and it is established that the convergence towards the maximum comes through the adjustment of its orientation under the following:

Proposition 1. *There is a functional with a local maximum (v_m) that is a function of the angles α, α_0 and β, β_0, such that it defines the increase in current through two rotations of the initial vector (v_0), one around the y-axis and the second around the z-axis, i.e.,*

$$v_m := M_y(\beta) \cdot M_z(\alpha) v_0 \tag{5}$$

with $M_z(\alpha)$ as a rotation matrix in z of angle α and $M_y(\beta)$ as a rotation matrix at y of angle β, which have the shape.

$$M_z(\alpha) := \begin{bmatrix} \cos(\alpha) & -\sin(\alpha) & 0 \\ \sin(\alpha) & \cos(\alpha) & 0 \\ 0 & 0 & 1 \end{bmatrix} \quad M_y(\beta) := \begin{bmatrix} \cos(\beta) & 0 & \sin(\beta) \\ 0 & 1 & 0 \\ -\sin(\beta) & 0 & \cos(\beta) \end{bmatrix}$$

Thus, replacing the $M_z(\alpha)$, $M_y(\beta)$ and v_0 in (5)

$$v_m = \begin{bmatrix} \cos(\alpha)\cos(\beta), & \sin(\alpha), & -\cos(\alpha)\sin(\beta) \end{bmatrix}^T$$

Similarly, we have

$$v_s = \begin{bmatrix} \cos(\alpha_0)\cos(\beta_0), & \sin(\alpha_0), & -\cos(\alpha_0)\sin(\beta_0) \end{bmatrix}^T$$

and because of this (4) can be seen as

$$i(\alpha, \beta) = YIS\|v_s\|\|v_m\|\cos(\theta) = YIS\cos(\theta) \tag{6}$$

Therefore, it is clear that if the value of θ (an auxiliary variable, representing the angle value between the unit vectors v_s and v_m) converges to 0, then the functional reaches a maximum and consequently (6) can be written based on this as:

$$\begin{aligned} i(\alpha, \beta) = YIS[\sin(\alpha_0)\sin(\alpha) + \cos(\alpha_0)\cos(\beta_0)\cos(\alpha)\cos(\beta) \\ + \cos(\alpha_0)\sin(b_0)\cos(\alpha)\sin(\beta)] \end{aligned} \tag{7}$$

2.3. ESC Algorithm

In a conventional configuration for a closed control loop (where the motors and SC that make up the ST are the plant), the current value of the current can be considered the output. The angular value of the position of the SC is the input and reference signal that results from the processing and modulation of the current. Therefore, a generalized diagram of the control circuit is presented in Figure 3.

It is important to mention that the operational components of the block called ESC correspond to the development of a cascade control scheme in whose outer loop the tasks of the ESC are carried out with the current readings of the SC. That is, its purpose is to optimize a certain function. On the other hand, a PI-type controller with anti-wind-up is executed in the internal loop to maintain the angle restrictions as well as avoid the accumulation effects of the integral action. The result of the operation of this control scheme allows the control efforts to be obtained, as well as to execute them on the motors. The above can be seen in greater detail in Figure 4. This controller architecture is robust and tuning is easy to implement [55]. In general, it is enough to have knowledge of the linear model of the servomechanism and develop a cascade linear control configuration.
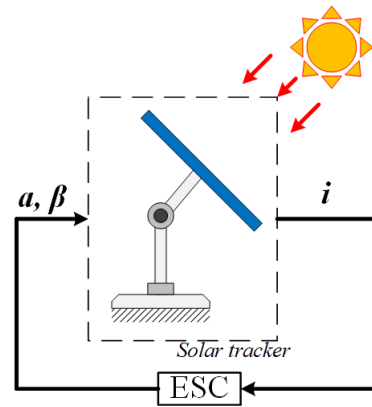
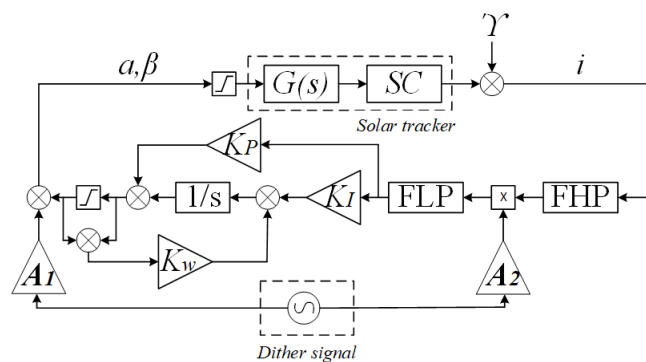**Figure 3.** General closed-loop scheme for ST with ESC.

Figure 4. Block diagram of ESC cascade control scheme.

From Figure 4, the terms $K_p = \text{diag}\{K_{p_1}, K_{p_2}\}$ and $K_{int} = \text{diag}\{K_{int_1}, K_{int_2}\}$ are matrices with proportional and integral gains, respectively. Then, $K_w = \text{diag}\{K_{w_1}, K_{w_2}\}$ is the calculation process matrix of the anti-wind-up system [56] and the saturation objects correspond to the angular constraints of the servomechanism expressed above. The rest of the components are explained as follows:

Proposition 2. *Let $f \colon \mathcal{A} \subseteq \mathbb{R}^n \to \mathbb{R}$ an at least twice differentiable and strongly convex functional on $\mathcal{A}$, where $\mathcal{A}$ is a convex subset, then, if there exists $x_0 \in \mathcal{A}$ such that $f(x_0) \leq f(x)$ for $x \in \mathcal{A} \backslash \{x_0\}$, it is possible to approximate the functional in a neighbourhood of radius $\epsilon > 0$ that contains x_0 as follows:*

$$f(x) \approx f(x_0) + \frac{1}{2}(x - x_0)^T \mathcal{H}(x_0)(x - x_0) \tag{8}$$

with $\mathcal{H}(x_0) > 0$, where $\mathcal{H}(\cdot)$ is the Hessian of the functional $f(\cdot)$. It is clear that $f(x_0)$ is the minimum of the functional.

Proof. This follows from the application of Taylor's Theorem for functions of several variables, which can be consulted in more detail in [32]. □

Theorem 1. *By the control scheme shown in Figure 4 and the functional proposed (7), the system is stable due to its active rejection of constant disturbances and converges to a region of the optimal point, such that it maximizes the functional.*

Proof. Extremum seeking is achieved by means of MIMO high-pass and low-pass filters (for this work called FHP and FLP, respectively), with the form

$$FHP := \frac{s}{s + w_h} \mathbb{I}_2, \quad FLP := \frac{w_l}{s + w_l} \mathbb{I}_2 \tag{9}$$

and a vector of synchronization disturbances (dither signal)

$$\delta(t) := \begin{bmatrix} a_1 \sin(w_1 t) & a_2 \sin(w_2 t) \end{bmatrix}^T \tag{10}$$

where $w_1, \ldots, w_n$ are sufficiently large frequencies such that $w_i \neq w_j$ with $i \neq j$ and $w_i + w_j \neq w_k$ for i, j, k distinct, $w_h \leq \min_n\{w_n\}$, $w_l < \min_n\{w_n\}$. The servomechanism has a transfer function $G(s)$, from the above, $G(s)$ can be considered as a filter with cutoff frequencies $\begin{bmatrix} \omega_{c_1} & \omega_{c_2} \end{bmatrix}^T$ [32]. This transfer function has as input the reference signals of the azimuthal and solar angles and exerts the electromechanical control actions necessary to reach them; the states $a \in [0, 2\pi)$ and $b \in \left[0, \frac{\pi}{2}\right]$ are stable equilibrium points of the system, since it is possible to reach them with this mechanism [57]. On another hand, from Proposition 1 the optimum that maximizes the current in the SC is $x_0 = (a_0, b_0)$ and the output of the PI controller with anti-wind-up presents an estimate $\check{x}$ of $x_0 = (a_0, b_0)$, which is added with the signal $\delta_1 = \begin{bmatrix} a_{11} \sin(w_1 t) & a_{12} \sin(w_2 t) \end{bmatrix}^T$. Thus, $\check{x} + \delta_1$ passes through the MIMO transfer function $G(s)$; for the analysis, it will be assumed that it is not saturated; later, we will apply the anti-wind-up technique to correct this assumption. So, the output of the servomechanism block will have the following signals: $G(s)\check{x} + \delta_1^*$, with $\delta_1^* = \begin{bmatrix} a_{13} \sin(w_1 t + \theta_1) & a_{14} \sin(w_2 t + \theta_2) \end{bmatrix}^T$, such that a_{13}, a_{14} are the amplitudes and θ_1, θ_2 are the phase shifts of the signal δ_1 passing through $G(s)$. It is possible to consider it as a filter with cutoff frequencies $\begin{bmatrix} \omega_{c_1} & \omega_{c_2} \end{bmatrix}^T$. At the input of the SC current with an angular perturbation $p(t) := (a_p, b_p) = p$ of constant type. From (7), the negative of it is taken with the idea of having a minimization problem, then the resulting Hessian evaluated at $x_0 = (a_0, b_0)$ is given by

$$\mathcal{H}(x_0) = \mathrm{Y}_i IS \begin{bmatrix} 1 & 0 \\ 0 & 1 - \sin^2(a_0) \end{bmatrix}$$

with $\mathcal{H}(x_0) \geq 0$ and to simplify the calculations $\tilde{x} := G(s)\check{x}$. Thus, applying Proposition 2, with $x = \delta_1^* - \hat{x} + x_0$ where $\hat{x} = x_0 - p - \tilde{x}$ and $\tilde{x}$ represents the angular output of the servomechanism, we have $i(\delta_1^* - \hat{x} + x_0) = i(x_0) + \frac{1}{2}(\delta_1^* - \hat{x})^T \mathcal{H}(x_0)(\delta_1^* - \hat{x})$, such that

$$i(\delta_1^* - \hat{x} + x_0) = [i(x_0) + \mathrm{Y}_i IS]\frac{1}{2}\hat{a}^2 - b_p\hat{b} - \frac{1}{2}\sin^2(a_0)\hat{b}^2 - \frac{1}{2}b_p^2\sin^2(a_0) + \frac{1}{2}\hat{b}^2 + \hat{b}b_p\sin^2(a_0)$$
$$+\frac{1}{2}a_{13}^2\sin^2(\theta_1)\cos^2(w_1 t) + \frac{1}{2}a_{13}^2\cos^2(\theta_1)\sin^2(w_1 t) + \frac{1}{2}a_{14}^2\sin^2(\theta_2)\cos^2(w_2 t) + \frac{1}{2}a_{14}^2\cos^2(\theta_2)\sin^2(w_2 t)$$
$$-\frac{1}{2}a_{14}^2\sin^2(a_0)\sin^2(\theta_2)\cos^2(w_2 t) - \frac{1}{2}a_{14}^2\sin^2(a_0)\cos^2(\theta_2)\sin^2(w_2 t) - a_{13}\hat{a}\kappa\cos(w_1 t) - a_{13}\hat{a}\iota\sin(w_1 t)$$
$$-a_{14}\hat{b}\varsigma\cos(w_2 t) - a_{14}\hat{b}\sigma\sin(w_2 t) + a_{13}^2\iota\kappa\cos(w_1 t)\sin(w_1 t) + a_{14}^2\sigma\varsigma\cos(w_2 t)\sin(w_2 t)$$
$$+a_{14}\hat{b}\sin^2(a_0)\varsigma\cos(w_2 t) + a_{14}\hat{b}\sin^2(a_0)\sigma\sin(w_2 t) - a_{14}\sin^2(a_0)\sigma\varsigma\cos(w_2 t)\sin(w_2 t)$$

with $\iota := \cos(\theta_1)$, $\kappa := \sin(\theta_1)$, $\sigma := \cos(\theta_2)$ and $\varsigma := \sin(\theta_2)$. On the other hand, if a signal analysis is performed, this function has a low frequency component, which can be eliminated by passing it through the FHP:

$$g := c_1 \cos(2w_1 t + \phi_1) + c_2 \cos(2w_2 t + \phi_2) + c_3\hat{a}\sin(w_1 t + \phi_3) + c_4\hat{b}\sin(w_2 t + \phi_4)$$

where $c_i > 0$ and $\phi_i > 0$ are the amplitude and phase changes of the signal when passing through the filter. The next step is to demodulate the signal by multiplying g by the vector $\delta_2 = \begin{bmatrix} a_{21} \sin(w_1 t) & a_{22} \sin(w_2 t) \end{bmatrix}^T$, that is

$$[g\delta_2]_1 = a_{21}\sin(w_1 t)[c_1\cos(2w_1 t + \phi_1) + c_2\cos(2w_2 t + \phi_2) + c_3\hat{a}\sin(w_1 t + \phi_3)$$
$$+c_4\hat{b}\sin(w_2 t + \phi_4)] = \frac{1}{2}a_{21}c_3\cos(\phi_3)\hat{a} + \mathcal{G}_1(w_1, w_2)$$

$$[g\delta_2]_2 = a_{22}\sin(w_2 t)[c_1\cos(2w_1 t + \phi_1) + c_2\cos(2w_2 t + \phi_2) + c_3\hat{a}\sin(w_1 t + \phi_3)$$
$$c_4\hat{b}\sin(w_2 t + \phi_4)] = \frac{1}{2}a_{22}c_4\cos(\phi_4)\hat{b} + \mathcal{G}_2(w_1, w_2)$$

with $\mathcal{G}_1(w_1, w_2)$ and $\mathcal{G}_2(w_1, w_2)$ functions containing trigonometric terms with multiples of the frequencies w_1 and w_2. Finally, this signal is passed through FLP and we obtain $h_1 := d_1 \hat{a}$ and $h_2 := d_2 \hat{b}$. These terms pass through the PI controller, which is considered to be in the non-saturation region, so, writing as operator:

$$\breve{a}(t) = \left[-K_{int_1} \int -K_{p_1}\right] d_1 \hat{a} \quad \text{and} \quad \breve{b}(t) = \left[-K_{int_2} \int -K_{p_2}\right] d_2 \hat{b}$$

with d_1 and d_2 being the amplitudes after passing through the filter, passing to the Laplace space and substituting we obtain:

$$\breve{a}(s) = d_1 \left(-K_{int_1} \frac{1}{s} - K_{p_1}\right) \left(a_0(s) - G_1(s)\breve{a}(s) - a_p(s)\right)$$
$$\breve{b}(s) = d_2 \left(-K_{int_2} \frac{1}{s} - K_{p_2}\right) \left(b_0(s) - G_2(s)\breve{b}(s) - b_p(s)\right)$$

Rewriting this, we have:

$$\breve{a}(s) = \frac{d_1 \left(K_{int_1} + K_{p_1} s\right) \left(\left(a_0(s) - a_p(s)\right)\right)}{K_{int_1} d_1 G_1(s) + K_{p_1} d_1 s G_1(s) - s}$$
$$\breve{b}(s) = \frac{d_2 \left(K_{int_2} + K_{p_2} s\right) \left(b_0(s) - b_p(s)\right)}{K_{int_2} d_2 G_2(s) + K_{p_2} d_2 s G_2(s) - s}$$

But because $\tilde{x} := G(s)\breve{x}$, we have that $\tilde{a}(s) = G_1(s)\breve{a}(s)$ and $\tilde{a}(s) = G_2(s)\breve{a}(s)$. Thus, substituting

$$\tilde{a}(s) = \frac{d_1 G_1(s) \left(K_{int_1} + K_{p_1} s\right) \left(a_0(s) - a_p(s)\right)}{K_{int_1} d_1 G_1(s) + K_{p_1} d_1 s G_1(s) - s}$$
$$\tilde{b}(s) = \frac{d_2 G_2(s) \left(K_{int_2} + K_{p_2} s\right) \left(b_0(s) - b_p(s)\right)}{K_{int_2} d_2 G_2(s) + K_{p_2} d_2 s G_2(s) - s}$$

Parameters for the PI are then chosen such that the previous transfer functions remain stable and additionally the estimated $\tilde{a}$ and $\tilde{b}$ have a small spectral content; that is, the cutoff frequency of this signal must be less than any other system signal. From the final value theorem, we have that, if $a_0(s) = a_0/s$ and $a_p(s) = a_p/s$, then:

$$\lim_{t \to \infty} \tilde{a}(t) = \lim_{s \to 0} s\tilde{a}(s) = a_0 - a_p$$

Similarly:

$$\lim_{t \to \infty} \tilde{b}(t) = \lim_{s \to 0} s\tilde{b}(s) = b_0 - b_p$$

Then $\lim_{t \to \infty} \tilde{x}(t) = x_0 - p$, and the angular input that the "PV cell current" block receives after a long time is given by $x = \delta_1^* - \hat{x} + x_0 = \delta_1^* - (x_0 - p - \tilde{x}) + x_0 = x_0 + \delta_1^*$. The first is a stationary state that converges to the optimum x_0; the second is a persistent state given by δ_1^*, which means that our system converges to a region of the optimum of radius $\max\{a_{11}, a_{12}\}$. Additionally, it was observed that it has active rejection of constant disturbances, so it can be considered as a robust controller. It is important to mention that these disturbances must be in the region where the angles are defined, otherwise, due to the presence of saturations, the controller would not have any effect. The previous theorem tells us that the control system operates perfectly in the linear region; however, to make an analysis in the saturation region, the following theorem is considered. $\square$

Theorem 2. *From the control scheme of Figure 4, the constant matrix K_w keeps the integrator unloaded, preventing the wind-up effect. Indeed, note that the saturation error e_s is zero when the system does not go into saturation; that is, the PI controller behaves linearly, but when the PI output exceeds the saturation values $e_s \neq 0$. In this way, suppose the steady state has been reached, then the saturation error is given by:*

$$e_s = \breve{x} - v$$

but:

$$v = -K_p e + \int (-K_{int} e - K_w e_s) dt$$

then:

$$e_s = \check{x} + K_p e + \int (K_{int}e + K_w e_s)dt$$

Taking the first derivative and considering the steady state, we have:

$$\dot{e}_s = K_{int}e + K_w e_s$$

So consider the Lyapunov function:

$$V = e_s^T P e_s$$

taking the first derivative:

$$\dot{V} = (K_{int}e + K_w e_s)^T P e_s + e_s^T P(K_{int}e + K_w e_s)$$
$$= e^T(K_{int}^T P + P^T K_w)e_s + e_s^T(K_w^T P + P^T K_w)e_s + e^T Q e - e^T Q e$$

with $P, Q > 0$ positive definite symmetric matrices. This problem is known as attractive ellipsoid [57]. Thus, the problem reduces to an LMI optimization problem [58].

The above problem can be simplified a little; ref. [59] suggests taking a value of K_w large enough so that the PI controller does not saturate.

3. Implementation and Experimental Test of ESC

To carry out the implementation and validation of the ESC in the ST, an experimental methodology was used that consisted of carrying out an energy-production test in real conditions, where the results are subjected to a comparative analysis concerning energy production with an SC in a fixed configuration. In this way, in addition to having a fair analysis in terms of performance, the profitability value of the proposal is also indirectly obtained. It is worth mentioning that to avoid bias in the comparative analysis process, the energy consumed by the ST itself is subtracted from the amount of energy produced by the ST. On the other hand, it is worth clarifying that for the proposal, as occurs in any other control scheme that is implemented in applications of this type, it is essential to have compliance with minimum operating conditions, which guarantees consistent operation, even helping reduce possible effects on profitability. For this reason, to carry out the ESC it must be considered that it is governed by an algorithm capable of managing the operation cycles. Figure 5 shows a generalized flowchart of the proposed algorithm, constantly monitoring the parameters associated with weather conditions and time, where M represents a generalized variable for the maintenance, adjustment and calibration management after the development of a certain number of operating cycles. Specifically, these parameters are acquired through a real-time clock module (model DS1307), a temperature and humidity sensor (model DHT11), and a barometric pressure sensor (model BMP180), respectively.
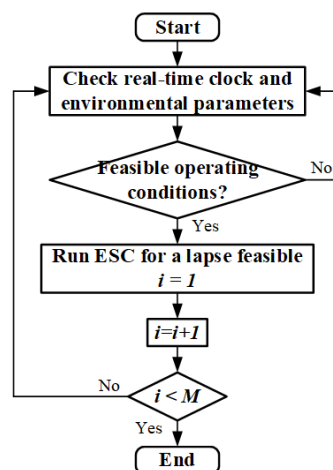

Figure 5. Flowchart of proposed algorithm for operating cycle management.

In general, the algorithm consists of guaranteeing the execution of the below two premises. First, that the operation period is feasible. That is, it is within the period between sunrise and sunset. And then, as part of a subdivision into shorter periods (between sunrise and sunset), it ensures that it is operated in favorable weather conditions since otherwise the system shuts down. Indirectly, the algorithm allows the energy consumption of the ST to be reduced, so that, in the event of inconvenient conditions, the ST will be forced to maintain a fixed orientation, which in operational terms implies producing the same as an SC in a fixed position. This occurs without incurring any expense since the motors used in the ST actuators can lock their last position (without the need for a power supply) thanks to the gear system that composes them.

Specifically, the performance test was carried out in the period between 8:00 a.m. and 5:00 p.m. on 6 February 2024, in the Applied Dynamic Systems Laboratory (located at UPIITA of the IPN in CDMX, with geographical coordinates 19.510736, −99.125897). The above is because the weather conditions that day were favorable (that is, mostly sunny and clear), although there were clouds present during certain periods, which made it possible to verify the robustness of the ESC and the performance of the cycle management algorithm of operation. It is worth mentioning that information about the conditions of the chosen day can be validated using the geographical coordinates of the laboratory location by consulting the database of sites such as [60]. Figure 6 shows the ST and fixed SC used in the test. The fixed SC was oriented following the recommendations of the technical literature used in the fixed installation of solar cells for generation purposes [61]. That is, in the azimuthal axis under the location of east and west, its center is oriented towards the south and in the elevation axis the surface is oriented using the value of the maximum angle (zenith) that it can reach during the day.

Figure 6. Fixed SC and ST used for performance test for ESC.

3.1. Configuration and Implementation of ESC program

To implement the ESC in the ST, Wayjung Toolbox was used, since this tool allows exporting symbolic programming (that is, high-level programming) directly from the ®Matlab-Simulink environment to the microcontroller. The above, with the aim of not losing sight of the fact that this proposal, in addition to showing the benefits of the ESC, is also capable of being put into practice simply. Therefore, the aspects related to its programming, as well as the subsequent adjustment and calibration tasks, manage to reduce its complexity and consequently this type of alternative can prevail among the viable options to take into account when following methodologies such as [16], whose objectives focus on the optimal selection of control laws for two-axis ST. Figure 7 shows the programming used for the microcontroller and is divided into three parts. Firstly, there is a microcontroller configuration block and another associated with the acquisition of the current sensor signal. Then, using conventional blocks, the ESC is developed. Specifically, this part has a direct equivalence to the diagram shown in Figure 4. Although, it can be

seen that the current signal is also used to determine the dynamics of the dither signal. Therefore, for this work it is proposed that in a practical way (10) takes the form

$$\delta(t) := \begin{bmatrix} a_1(t)\sin(w_1 t) & a_2(t)\sin(w_2 t) \end{bmatrix}^T$$

such that, for the period between sunrise and zenith a_n is given by

$$a_n = \begin{cases} a, & i(t-1) < i(t) \\ 0, & i(t-1) \geq i(t) \end{cases}$$

where a represents a generalized variable that is associated with the minimum amplitude that the dither signal must have to mobilize each axis. This proposal was made taking into account that the solar trajectory evolves with changes of 1 degree every four minutes (in one or both axes) and that in this period (from dawn to zenith) the energy production must maintain an increasing behavior. Furthermore, if an SC has on average an acceptance angle of $\pm 2°$, for which it can maintain its maximum production rate [7], then in practice it is not necessary that the ESC maintain continuous operation since the energy-generation dynamics can remain with some similarity in periods of up to 8 min. On the other hand, for the period from zenith to sunset a_n has the form

$$a_n = \begin{cases} a, & i(t-1) \neq i(t) \\ 0, & i(t-1) = i(t) \end{cases}$$

It is important to mention that in the operation of the ESC and specifically in the construction of the dither signal, the parameter t is subject to the development of the microcontroller's operating time, since ultimately it is this device where it is executed and whose value is 0.001 s. Therefore, it can be established that this proposal does not compromise the convergence of the calculation of the optimal value solution in real time. That is, physically it can be observed that the ST remains motionless, although every 0.001 s it makes the decision to update the last position. On the other hand, by using special ®Waijung blocks, the control signals are processed to be interpreted externally using the VNH2SP30 controller. For more information on ®Waijung blocks, as well as technical considerations for their configuration, see [62]. To validate the contributions provided by the operation cycle management algorithm and the construction of the dither signal according to the dynamics of solar irradiance, a test was developed with similar characteristics to those of the case study, although without such restrictions. That is, monitor and compare the performance of the free operation of the ST and the fixed SC during a period (12:15 to 1:15 p.m. on 13 February 2024) in which adverse weather conditions are associated with a forecast of rain. The results of this test are shown in Appendix B.

For the configuration and tuning of the ESC, the value of the gains and/or parameters used are $K_{p_1} = 18$, $K_{int_1} = 1$ and $K_{p_2} = 60$, $K_{int_2} = 1$ for the PI controller corresponding to the azimuthal and elevation mechanism, respectively. Then, $w_h = 2$, $w_l = 1.5$. This considers that the operating frequency of each motor is $w_{c1} = w_{c2} = 3.14 \frac{rad}{seg}$ (for more details consult the technical sheet [63]). Furthermore, $w_1 = w_2 = 0.039$ is the result of using the relationship $w = 2\pi f$, with f as the frequency of a signal (solar trajectory) with significant changes every 0.25 s (i.e., $T = 0.25$, for $f = \frac{1}{T}$). On the other hand, for the anti-wind-up effect $k_w = 4$. It is worth mentioning that the values of K_p, K_{int} (of each controller), w_h, w_l and k_w were obtained heuristically under an offline tuning process, which is based on the development of the following fundamental stages:

- Initiation of parameters and controller gains: from the technical sheets of the motors (to determine their parameters), the proposal of safe values for the PI controller and the analysis of the development time of the tasks, an initial configuration of the ESC is established.
- Test controller and performance monitoring: ST pointing tests are carried out for short periods and through an analysis of the tracking error value, as well as the operation of management system routines, the gain value is updated, until the error value is within the admissible limit. Therefore, it must be taken into account that in the tuning process, the aim is not to perfectly align the SC with the sun, since that would not imply any difference in production; it only seeks to comply with the requirement guaranteed by the MPPT.
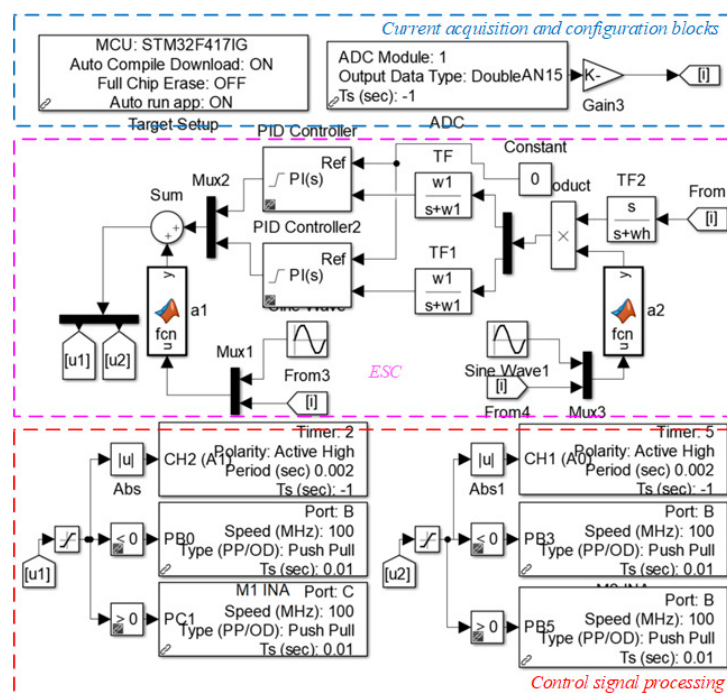
Figure 7. ESC program, in ®Matlab-Simulink environment.

In operational terms, given that the maximum production region of the SC is wide, it allows gains to be obtained with a certain flexibility. Otherwise, increasing and/or over-tuning them implies, due to the nature of the controller, having more and greater control efforts, which in the end is a higher energy consumption. On the other hand, it should not be forgotten that the general control scheme operates under a cascade configuration, so the ESC allows for overcoming deficiencies and converging to the optimum. Finally, it is natural to consider that the values of the parameters that represent the ST will change, either due to wear effects, or due to the operation itself, so the process also involves the development of tasks associated with the resolution of this type of problem. For more details on the process, as well as the considerations that must be taken into account for its development, consult the tuning process section reported in [7].

3.2. Experimental Results

Figure 8 graphically shows the results obtained in terms of energy production of the ST and the fixed SC. Specifically, the upper graph shows the power generated, which is the resulting product of the current and voltage measurements of each SC, while the lower graph shows an equivalence in terms of the accumulated energy it represents. Then, as complementary elements, Figure 9 shows the results of the tracking error generated by the MEMS. This is with the purpose of recording and visualizing the performance of the ESC, as well as the operation cycle management algorithm and the construction dynamics

of the dither signal, since the MEMS sensor is a device that allows measuring the solar pointing error with 99.97 % concerning the position in which it is oriented. The MEMS sensor can be seen as a standard element that records the precision with which the ST is oriented, which indirectly also implies knowing the operating dynamics of the ESC.
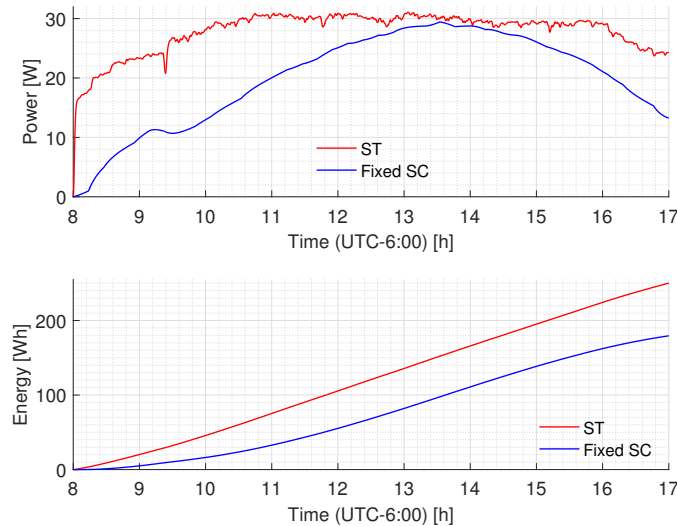

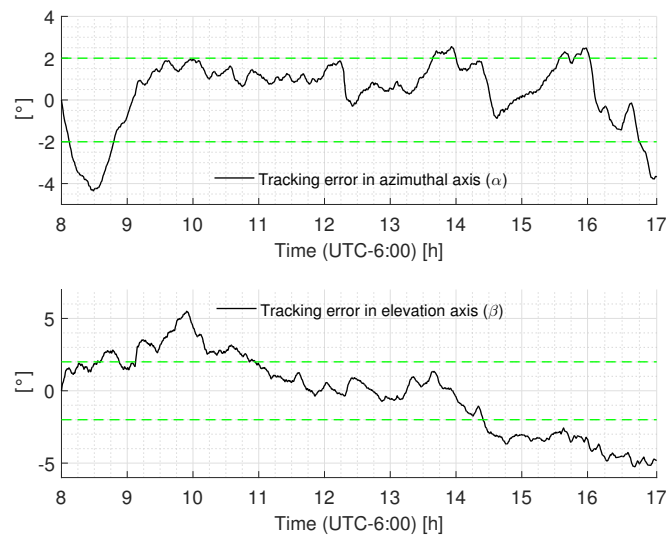**Figure 8.** Graphic results of energy production.

Figure 9. Graphic results of tracking error. In the figure, the acronym TEAA is tracking error in azimuthal axis and TEEA is tracking error in elevation axis.

The graphical data are also presented numerically through Tables 1 and 2 to simplify the results and facilitate subsequent analysis. In particular, for Table 1, the first column shows the numerical value of the energy accumulated through the ST and the fixed SC. The second column shows the value of the energy consumed (if applicable) and the third column shows the energy resulting. That is the final value of the available energy after subtracting the value of the energy consumed from the value of the accumulated energy. On the other hand, Table 2 presents in columns one and two the value of the average absolute error in each axis, which is given by $AAVTE_n = \sum_1^N \frac{|E_n(N)|}{N}$, for $n = 1, 2$, where each value of n is associated with the tracking error signal for the azimuthal and elevation axes, respectively, and N is the total number of samples that compose each signal. Finally, in the third column, the value of the mixed error (ME) is shown, which is the result of calculating the average of the previous two (i.e., $ME = \frac{AAVTE_1 + AAVTE_2}{2}$).

Table 1. Numerical results of energy production. In the table, the acronym AcE is accumulated energy, ECo is energy consumed, FEV is final energy value and N/A means does not apply.

System	AcE (Wh)	ECo (Wh)	FEV (Wh)
ST	250.2	21	229.2
Fixed SC	179.4	NA	179.4

Table 2. Numerical results of tracking error. In the table, the acronym AAVTE is average absolute value of tracking error and the subscript is associated with the azimuthal and elevation axes, respectively, and ME is mixed error.

$AAVTE_1$ (°)	$AAVTE_2$ (°)	ME (°)
1.3543	2.2373	1.8636

Another way to interpret the dynamics of the tracking error is through Figure 10 and Table 3. The figure has a graphical representation of the normalized occurrence error (NOE) value on each axis (i.e., a histogram) and the table shows the percentage value of the NOE concerning the tolerance band (shown in yellow) that is associated with the acceptance angle of the SC. In this way, both elements allow a brief statistical analysis of the trend in the angular error produced by the ESC in the ST.
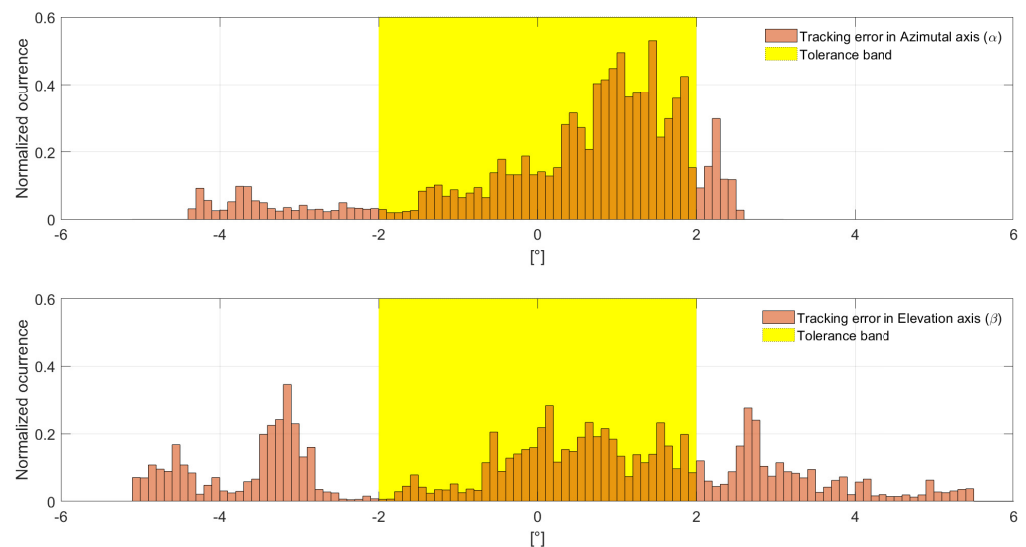
Figure 10. Normalized occurrence error.

Table 3. Percentage value of the normalized occurrence error (NOE) concerning the tolerance band. In the table, NOE_1 is associated with the azimuthal axis and NOE_2 with the elevation axis

NOE_1 (%)	NOE_2 (%)
81.5	47.3

3.3. Analysis of Results and Discussion

Through Figure 8, it can be observed that the ST had a better use of solar radiation than the fixed system. This is specifically in the periods close to sunrise and sunset since it is evident that there is a greater production. The results make evident the amount of energy that a fixed system manages to waste, or, for this work, the value of the unnecessary collection surface, which has an approximate value in ideal terms of 40% (without subtracting the power consumed by the ST), or a real value of 27.75% (according to Table 1). In other words, the proposal allows for a real gain in production of 27.75%, which is a transcendental fact,

since according to [64] (a review of methods to maximize solar systems), the gains offered by real systems range from 10 to 20% and higher values are only achieved in theoretical systems that are tested under experimental scenarios in controlled environments and/or purely in simulation environments.

In general, production results can be linked to ESC performance, which can be analyzed through tracking error dynamics. For example, in Figure 9 it is evident that the curves on each axis were largely developed within the permissible region (or a close neighborhood) for the SC to maintain its maximum production regime, since the pointing accuracy obtained had a deviation value of 1.8636° (according to Table 2), which is feasible since the SC has an acceptance angle or tolerance band of $\pm2°$. However, it is important to establish that according to the results of Figure 10 and Table 3, although it is evident that the occurrence of the error values is largely contained within the tolerance band (mainly in the azimuthal axis which has 81.5%), its distribution is not uniform and particularly in the case of the elevation axis there is a low percentage with a value of 47.3%, which can be interpreted as part of the demand that one axis suffers more than another. That is, in the elevation axis the effects of disturbances associated with external dynamics such as wind, gravity effects and dead zones in the engine and its mechanisms, among others, are more present than in the azimuthal axis and therefore the error dynamics have more significant values, which can be associated with greater control efforts.

Thus, from the above it can be established that the ESC maintains an admissible precision and its performance is competitive with respect to systems that act with the same purposes and although it is natural that its operation does not have a uniform distribution in the control actions, it is important to mention that this does not greatly affect its performance. In fact, while it is true that it is desirable to reduce these effects, at the same time the effectiveness of the ESC is demonstrated because even when the ST is not a perfect system (in mechanical terms) and its modeling has uncertainties, it is still guaranteed to reach the optimum. In this way, it becomes easy to assume and validate the robustness of the algorithm since it is evident that the convergence to the optimum occurs independently of the variation of the parameters of the ST, as long as the changes do not imply exceeding admissible limits that compromise the resolution and/or favorable conditions in the mechanisms that compose it. Therefore, PI-type controllers that govern control efforts indirectly can remain with simple configurations, in which it is not necessary to use high gain schemes and/or make continuous changes in their tuning.

4. Conclusions and Future Work

A new control strategy based on extremum-seeking control for solar tracking systems is proposed, implemented and tested to increase the production efficiency of photovoltaic technology. In addition, it allows the reduction of the wear of the tracker actuators and mechanisms due to the control action. The proposal is validated through an experimentation process and compared with a fixed configuration, increasing the production efficiency by 27.5%. Consequently, the solar collection surface can be reduced in solar farms without affecting the generation capacity. Additionally, the tracking error obtained is 1.8636°, which is less than the recommended value of 2° for conventional photovoltaic technology. Starting from the operating cycle management system, the dither signal algorithm and the anti-wind-up, the ST managed to maintain uninterrupted operation for 9 h with 21 Wh energy consumption. Which represents 8.39% of the amount of energy produced, and based on [64], the proposal is a viable and competitive alternative compared to commercial systems. On the other hand, the implementation of the strategy on a microcontroller through the ToolBox ®Waijung allows for reducing the complexity of the task configuration and monitoring process. Finally, this research allows future developments of more efficient solar harvesting systems and consequently reduces the collection surface required for a defined energy requirement.

In future work, pointing accuracy can be improved by adjusting controller gains and parameters with functions built in real time through philosophies based on optimization schemes and adaptive laws, including the development of parameter-identification schemes that allow obtaining models closer to the reality of the ST and the SC.

Appendix A. Experimental Estimation of Y

As a complement to the monitoring during the development of the ESC performance test, information was obtained from the pyrheliometer and pyranometer measurements (see Figure A1). This is to know the ideal value of power production (and consequently, energy) that a mobile and fixed system can produce (in this case, the ST and fixed SC used). Then, taking into account that both results are associated with the following units $\frac{W}{m^2}$ or $\frac{Wh}{m^2}$, it is enough to calculate the difference that was obtained in the performance of each system (contained in Table 1) and equalize the surface. That is, a solar cell like the ones used in this case study has an approximate surface area of 0.198 m^2. Therefore, to equalize the surface and be able to compare with the instrument values, the results are multiplied with a value of 5.05. Table A1 shows the numerical results of this process. Where it is easy to see that the energy of the ST represents 20.16% of the ideal value represented by the pyrheliometer, while the energy value of the fixed SC is 20.62% of the ideal value represented by the pyranometer. Thus, the value of Y is proposed to be the average, that is, 20.39% or 0.2039 to give continuity to the development of the modeling process in the Section 2.2.

Table A1. Numerical results of accumulated energy of pyrheliometer, pyranometer, ST and fixed SC. For ST and SC fixed, the value presented is the result of multiplying the test results (contained in Table 1) by 5.05 to equalize the surface to 1 m^2.

| System	Energy (Wh/m^2)
Pyrheliometer	6266
Pyranometer	4393
ST	1263.51
Fixed SC	905.97
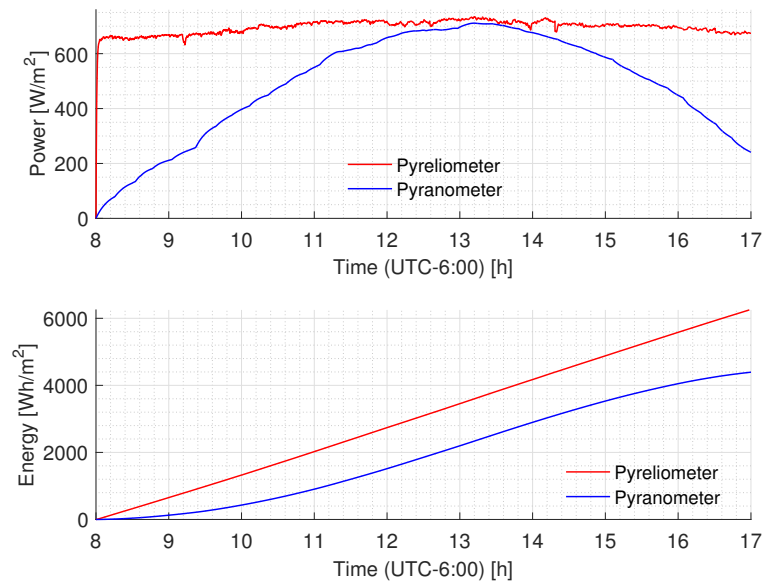
Figure A1. Graphic results of pyrheliometer and pyranometer measurements and monitoring during test development.

Appendix B. Test in Adverse Weather Conditions

Figures A2 and A3 show the graphical results and Tables A2 and A3 their numerical equivalence (so the calculations of FEV and ME are derived from the follow-up of the operations defined in Section 3.2). In these, it can be easily noted that although the ST managed to locate in some cases the best trajectory for direct solar radiation, for productive purposes there is no significant difference. Furthermore, if the value consumed by the ST is subtracted from the energy produced, the proposal loses profitability since its final production is lower (approximately 84.38%) compared to that of the fixed SC. On the other hand, it should be noted that the operation of the MEMS sensor implies having a minimum value of 300 $\frac{W}{m^2}$ of solar irradiance. Thus, in the tracking error graph there is a period without information, although it must be understood that it has the same dynamics as the rest of the data.
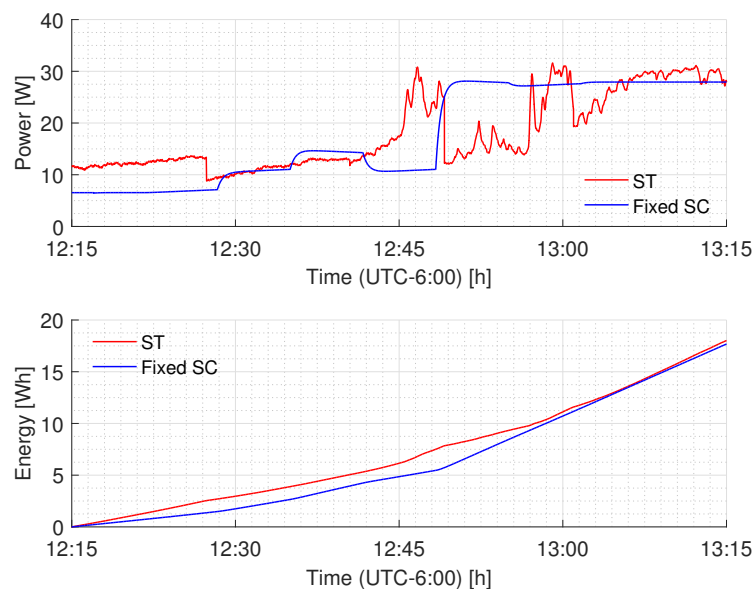
Figure A2. Graphic results of energy production of the test in adverse weather conditions.
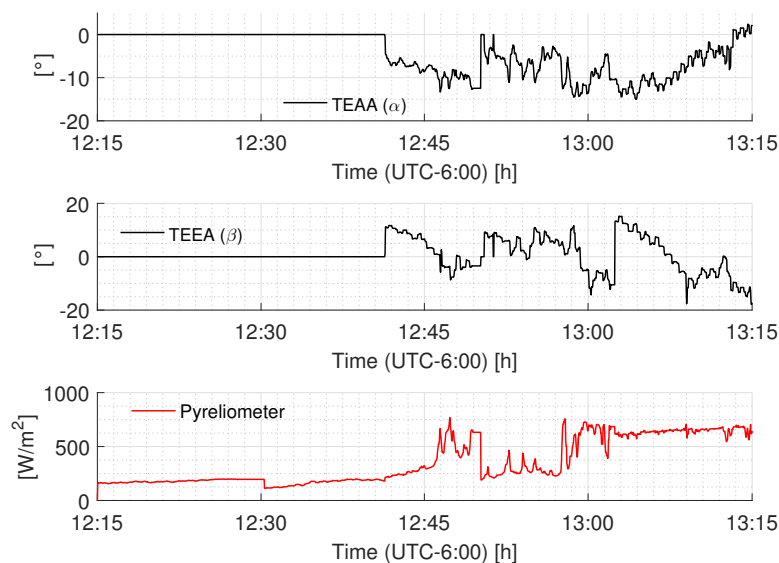
Figure A3. Graphic results of tracking error of test in adverse weather conditions. In the figure, the acronym TEAA is tracking error in azimuthal axis and TEEA is tracking error in elevation axis.

Table A2. Energy production numerical results of test in adverse weather conditions. In the table, the acronym AcE is accumulated energy, ECo is energy consumed, FEV is final energy value and N/A means does not apply.

System	AcE (Wh)	ECo (Wh)	FEV (Wh)
ST	18.02	3.1	14.92
Fixed SC	17.68	N/A	17.68

Table A3. Tracking error numerical results of test in adverse weather conditions. In the table, the acronym AAVTE is average absolute value of tracking error and the subscript is associated with the azimuthal and elevation axes, respectively, and ME is mixed error

AAVTE in α (°)	AAVTE in β (°)	ME (°)
4.3536	3.7669	4.0602

References

1. Kanoğlu, M.; Çengel, Y.A.; Cimbala, J.M. *Fundamentals and Applications of Renewable Energy*; McGraw-Hill Education: New York, NY, USA, 2020.
2. U.S. Energy Information Administration, USA. Available online: https://www.eia.gov (accessed on 8 October 2023).
3. Iqbal, M. *An Introduction to Solar Radiation*; Elsevier: Amsterdam, The Netherlands, 2012.
4. Abou Jieb, Y.; Hossain, E.; Hossain, E. *Photovoltaic Systems: Fundamentals and Applications*; Springer: Berlin/Heidelberg, Germany, 2022.
5. Prinsloo, G.; Dobson, R. *Sun Tracking and Solar Renewable Energy Harvesting: Solar Energy Harvesting, Trough, Pinpointing and Heliostat Solar Collecting Systems*; Solar Books: Stellenbosch, South Africa, 2015; pp. 1–542. ISBN 978Y0Y620Y61576Y1.
6. Leutz, R.; Suzuki, A. *Nonimaging Fresnel Lenses: Design and Performance of Solar Concentrators*; Springer: Berlin/Heidelberg, Germany, 2012; Volume 83.
7. Palomino-Resendiz, S.; Flores-Hernández, D.; Cantera-Cantera, L.; Lozada-Castillo, N.; Luviano-Juárez, A. Design and implementation of Model-Based Predictive Control for two-axis Solar Tracker. *Sol. Energy* **2023**, *265*, 112080. [CrossRef]
8. Alam, M.A.; Khan, M.R. *Principles of Solar Cells: Connecting Perspectives on Device, System, Reliability and Data Science*; World Scientific: Singapore, 2022.
9. Angulo-Calderón, M.; Salgado-Tránsito, I.; Trejo-Zúñiga, I.; Paredes-Orta, C.; Kesthkar, S.; Díaz-Ponce, A. Development and accuracy assessment of a high-precision dual-axis pre-commercial solar tracker for concentrating photovoltaic modules. *Appl. Sci.* **2022**, *12*, 2625. [CrossRef]
10. Chowdhury, M.S.; Rahman, K.S.; Chowdhury, T.; Nuthammachot, N.; Techato, K.; Akhtaruzzaman, M.; Tiong, S.K.; Sopian, K.; Amin, N. An overview of solar photovoltaic panels' end-of-life material recycling. *Energy Strategy Rev.* **2020**, *27*, 100431. [CrossRef]

11. Xu, Y.; Li, J.; Tan, Q.; Peters, A.L.; Yang, C. Global status of recycling waste solar panels: A review. *Waste Manag.* **2018**, *75*, 450–458. [CrossRef]
12. Turney, D.; Fthenakis, V. Environmental impacts from the installation and operation of large-scale solar power plants. *Renew. Sustain. Energy Rev.* **2011**, *15*, 3261–3270. [CrossRef]
13. Huang, W.H.; Shin, W.J.; Wang, L.; Sun, W.C.; Tao, M. Strategy and technology to recycle wafer-silicon solar modules. *Sol. Energy* **2017**, *144*, 22–31. [CrossRef]
14. Flores-Hernández, D.; Palomino-Resendiz, S.; Lozada-Castillo, N.; Luviano-Juárez, A.; Chairez, I. Mechatronic design and implementation of a two axes sun tracking photovoltaic system driven by a robotic sensor. *Mechatronics* **2017**, *47*, 148–159. [CrossRef]
15. Flores-Hernández, D.A.; Palomino-Resendiz, S.I.; Luviano-Juárez, A.; Lozada-Castillo, N.; Gutierrez-Frias, O. A heuristic approach for tracking error and energy consumption minimization in solar tracking systems. *IEEE Access* **2019**, *7*, 52755–52768. [CrossRef]
16. Palomino-Resendiz, S.I.; Ortiz-Martínez, F.A.; Paramo-Ortega, I.V.; González-Lira, J.M.; Flores-Hernández, D.A. Optimal Selection of the Control Strategy for Dual-Axis Solar Tracking Systems. *IEEE Access* **2023**. [CrossRef]
17. Ozcelik, S.; Prakash, H.; Challoo, R. Two-axis solar tracker analysis and control for maximum power generation. *Procedia Comput. Sci.* **2011**, *6*, 457–462. [CrossRef]
18. Fam, D.; Koh, S.; Kiong, T.S.; Chong, K.H. Optimization variation for multiple heuristic approaches in solar tracking. *Key Eng. Mater.* **2011**, *480*, 1085–1090. [CrossRef]
19. Verma, P.; Alam, A.; Sarwar, A.; Tariq, M.; Vahedi, H.; Gupta, D.; Ahmad, S.; Shah Noor Mohamed, A. Meta-heuristic optimization techniques used for maximum power point tracking in solar pv system. *Electronics* **2021**, *10*, 2419. [CrossRef]
20. Alrubaie, A.J.; Al-Khaykan, A.; Malik, R.; Talib, S.H.; Mousa, M.I.; Kadhim, A.M. Review on MPPT techniques in solar system. In Proceedings of the 2022 8th International Engineering Conference on Sustainable Technology and Development (IEC). IEEE, Erbil, Iraq, 23–24 February 2022; pp. 123–128.
21. Ali, A.N.A.; Saied, M.H.; Mostafa, M.Z.; Abdel-Moneim, T.M. A survey of maximum PPT techniques of PV systems. In Proceedings of the 2012 IEEE Energytech, Cleveland, OH, USA, 29–31 May 2012; pp. 1–17.
22. Karami, N.; Moubayed, N.; Outbib, R. General review and classification of different MPPT Techniques. *Renew. Sustain. Energy Rev.* **2017**, *68*, 1–18. [CrossRef]
23. Palomino-Resendiz, S.I.; Flores-Hernández, D.A.; Lozada-Castillo, N.; Luviano-Juárez, A. High-precision luminosity sensor for solar applications. *IEEE Sens. J.* **2019**, *19*, 12454–12464. [CrossRef]
24. Amir, A.; Selvaraj, J.; Rahim, N.A. Study of the MPP tracking algorithms: Focusing the numerical method techniques. *Renew. Sustain. Energy Rev.* **2016**, *62*, 350–371. [CrossRef]
25. Podder, A.K.; Roy, N.K.; Pota, H.R. MPPT methods for solar PV systems: A critical review based on tracking nature. *IET Renew. Power Gener.* **2019**, *13*, 1615–1632. [CrossRef]
26. Tina, G.M.; Arcidiacono, F.; Gagliano, A. Intelligent sun-tracking system based on multiple photodiode sensors for maximisation of photovoltaic energy production. *Math. Comput. Simul.* **2013**, *91*, 16–28. [CrossRef]
27. Kasa, N.; Iida, T.; Chen, L. Flyback inverter controlled by sensorless current MPPT for photovoltaic power system. *IEEE Trans. Ind. Electron.* **2005**, *52*, 1145–1152. [CrossRef]
28. Salgado-Conrado, L. A review on sun position sensors used in solar applications. *Renew. Sustain. Energy Rev.* **2018**, *82*, 2128–2146. [CrossRef]
29. Averbukh, M.; Ben-Galim, Y.; Uhananov, A. Development of a quick dynamic response maximum power point tracking algorithm for off-grid system with adaptive switching (On–Off) control of dc/dc converter. *J. Sol. Energy Eng.* **2013**, *135*, 021003. [CrossRef]
30. Khaled, A.; Aboubakeur, H.; Mohamed, B.; Nabil, A. A fast MPPT control technique using PID controller in a photovoltaic system. In Proceedings of the 2018 International Conference on Applied Smart Systems (ICASS), Medea, Algeria, 24–25 November 2018; pp. 1–5.
31. Harrag, A.; Messalti, S. Variable step size modified P&O MPPT algorithm using GA-based hybrid offline/online PID controller. *Renew. Sustain. Energy Rev.* **2015**, *49*, 1247–1260.
32. Ariyur, K.B.; Krstic, M. *Real-Time Optimization by Extremum-Seeking Control*; John Wiley & Sons: Hoboken, NJ, USA, 2003.
33. Katsanikakis, A.; Bechlioulis, C.P. Design and Implementation of an Energy-Efficient Vehicle Platoon Control Algorithm Using Prescribed Performance and Extremum Seeking Control. *Appl. Sci.* **2023**, *13*, 5650. [CrossRef]
34. Krstic, M.; Ghaffari, A.; Seshagiri, S. Extremum seeking for wind and solar energy applications. In Proceedings of the 11th World Congress on Intelligent Control and Automation, Shenyang, China, 29 June–4 July 2014; pp. 6184–6193.
35. Leyva, R.; Alonso, C.; Queinnec, I.; Cid-Pastor, A.; Lagrange, D.; Martinez-Salamero, L. MPPT of photovoltaic systems using extremum-seeking control. *IEEE Trans. Aerosp. Electron. Syst.* **2006**, *42*, 249–258. [CrossRef]
36. Tan, Y.; Moase, W.H.; Manzie, C.; Nešić, D.; Mareels, I.M. Extremum seeking from 1922 to 2010. In Proceedings of the 29th Chinese Control Conference, Beijing, China, 29–31 July 2010; pp. 14–26.
37. Metry, M.; Shadmand, M.B.; Balog, R.S.; Abu-Rub, H. MPPT of photovoltaic systems using sensorless current-based model predictive control. *IEEE Trans. Ind. Appl.* **2016**, *53*, 1157–1167. [CrossRef]

38. Fatemi, S.M.; Shadlu, M.S.; Talebkhah, A. A new method for maximum power point tracking in solar PV systems by combining extremum seeking method (ESM) and model predictive control (MPC). In Proceedings of the 2020 11th Power Electronics, Drive Systems and Technologies Conference (PEDSTC), Tehran, Iran, 4–6 February 2020; pp. 1–5.

39. Moura, S.J.; Chang, Y.A. Lyapunov-based switched extremum seeking for photovoltaic power maximization. *Control Eng. Pract.* **2013**, *21*, 971–980. [CrossRef]

40. Zou, Y.; Tan, W.; Jin, X.; Wang, Z. An active disturbance rejection control of large wind turbine pitch angle based on extremum-seeking algorithm. *Energies* **2022**, *15*, 2846. [CrossRef]

41. Sahu, J.K.; Mishra, S.K.; Patra, J.P. MPPT Extremum Seeking Control Algorithm for Standalone PV System. In Proceedings of the 2023 5th International Conference on Smart Systems and Inventive Technology (ICSSIT), Tirunelveli, India, 23–25 January 2023; pp. 156–160.

42. Senthilkumar, S.; Mohan, V.; Deepa, R.; Nuthal Srinivasan, M.; Senthil Kumar, T.; Thanikanti, S.; Prathap, N. A review on MPPT algorithms for solar PV systems. *Int. J. Res. Granthaalayah* **2023**, *11*, 25–64. [CrossRef]

43. Bizon, N. Global Maximum Power Point Tracking (GMPPT) of Photovoltaic array using the Extremum Seeking Control (ESC): A review and a new GMPPT ESC scheme. *Renew. Sustain. Energy Rev.* **2016**, *57*, 524–539. [CrossRef]

44. Bratcu, A.I.; Munteanu, I.; Bacha, S.; Raison, B. Maximum power point tracking of grid-connected photovoltaic arrays by using extremum seeking control. *J. Control Eng. Appl. Inform.* **2008**, *10*, 3–12.

45. Heydari-doostabad, H.; Keypour, R.; Khalghani, M.R.; Khooban, M.H. A new approach in MPPT for photovoltaic array based on extremum seeking control under uniform and non-uniform irradiances. *Sol. Energy* **2013**, *94*, 28–36. [CrossRef]

46. Menadi, A.; Boukahil, F.Z.; Betka, A. Real-Time Implementation of a Hybrid ESC Approach for Maximising the Extracted Photovoltaic Power Under Partial Shading Conditions. *Power Electron. Drives* **2024**, *9*, 191–204. [CrossRef]

47. Rasheed, M.; Shihab, S. Analytical Modeling of Solar Cells. *Insight-Electronic* **2019**. [CrossRef]

48. Álvarez, J.M.; Alfonso-Corcuera, D.; Roibás-Millán, E.; Cubas, J.; Cubero-Estalrrich, J.; Gonzalez-Estrada, A.; Jado-Puente, R.; Sanabria-Pinzón, M.; Pindado, S. Analytical modeling of current-voltage photovoltaic performance: An easy approach to solar panel behavior. *Appl. Sci.* **2021**, *11*, 4250. [CrossRef]

49. Amajama, J. Effect of Solar Illuminance (or Intensity) on Solar (Photovoltaic) cell's output and the use of Converging lenses and X or Gamma rays to enhance output performance. *Int. J. Eng. Res. Gen. Sci.* **2016**, *4*, 284–289.

50. Smestad, G.; Ries, H. Luminescence and current-voltage characteristics of solar cells and optoelectronic devices. *Sol. Energy Mater. Sol. Cells* **1992**, *25*, 51–71. [CrossRef]

51. Hayat, M.B.; Ali, D.; Monyake, K.C.; Alagha, L.; Ahmed, N. Solar energy—A look into power generation, challenges and a solar-powered future. *Int. J. Energy Res.* **2019**, *43*, 1049–1067. [CrossRef]

52. Wang, A.; Xuan, Y. A detailed study on loss processes in solar cells. *Energy* **2018**, *144*, 490–500. [CrossRef]

53. Keitz, H.; Keitz, H. Luminous Flux, Luminous Intensity, Quantity of Light. In *Light Calculations and Measurements: An Introduction to the System of Quantities and Units in Light-Technology and to Photometry*; Red Globe Press London: London, UK, 1971. Available online: https://link.springer.com/book/10.1007/978-1-349-00012-8 (accessed on 9 February 2024).

54. WILSON, D. BASIC SERVOMECHANISM THEORY. *Mod. Pract. Servo Des. Int. Ser. Monogr. Electr. Eng.* **2013**, *2*, 1.

55. Azar, A.T.; Serrano, F.E. Design and modeling of anti wind up PID controllers. In *Complex System Modelling and Control through Intelligent Soft Computations*; Springer: Berlin/Heidelberg, Germany, 2014; pp. 1–44.

56. Glattfelder, A.; Schaufelberger, W. Start-up performance of different proportional-integral-anti-wind-up regulators. *Int. J. Control* **1986**, *44*, 493–505. [CrossRef]

57. Poznyak, A.S. *Advanced Mathematical Tools for Control Engineers: Volume 1: Deterministic Systems*; Elsevier: Amsterdam, The Netherlands, 2010; Volume 1,

58. Boyd, S.; El Ghaoui, L.; Feron, E.; Balakrishnan, V. *Linear Matrix Inequalities in System and Control Theory*; SIAM: Philadelphia, PA, USA, 1994.

59. Bucz, Š.; Kozáková, A. Advanced methods of PID controller tuning for specified performance. *PID Control Ind. Process.* **2018**, 73–119. [CrossRef]

60. AccuWeather. Available online: https://www.accuweather.com/ (accessed on 9 February 2024).

61. Martín, P.F.G. *Energía Solar Fotovoltaica Para Todos*; Marcombo: Barcelona, Spain, 2021.

62. Waijung Blockset. Available online: https://waijung1.aimagin.com/ (accessed on 9 February 2024).

63. Gobilda. Available online: https://www.gobilda.com/ (accessed on 9 February 2024).

64. Mousazadeh, H.; Keyhani, A.; Javadi, A.; Mobli, H.; Abrinia, K.; Sharifi, A. A review of principle and sun-tracking methods for maximizing solar systems output. *Renew. Sustain. Energy Rev.* **2009**, *13*, 1800–1818. [CrossRef]